Fractals, Vol. 15, No. 1 (2007) 27–39

World Scientific
www.worldscientific.com

A SIMPLIFIED ANALYTICAL MODEL FOR LAPLACIAN TRANSFER ACROSS DETERMINISTIC PREFRACTAL INTERFACES

D. S. GREBENKOV,*,‡ M. FILOCHE*,† and B. SAPOVAL*,†
*Laboratoire de Physique de la Matière Condensée
C. N. R. S.—Ecole Polytechnique, 91128 Palaiseau, France
†Centre de Mathématiques et de leurs Applications, C. N. R. S.
Ecole Normale Supérieure, 94140 Cachan, France
‡denis.grebenkov@polytechnique.edu

Received January 30, 2006
Accepted August 26, 2006

Abstract

The role of the geometry of prefractal interfaces in Laplacian transport is analyzed through its "harmonic geometrical spectrum." This spectrum summarizes the properties of the Dirichlet-to-Neumann operator associated with these geometries. Numerical analysis shows that very few eigenmodes contribute significantly to the macroscopic response of the system. The hierarchical spatial frequencies of these particular modes correspond to the characteristic length scales of the interface. From this result, a simplified analytical model of the response of self-similar interfaces is developed. This model reproduces the classical low and high frequency asymptotic limits and gives an approximate constant phase angle behavior for the intermediate frequency region. It also provides an analytical description for the crossovers between these regimes and for their dependency on the order of the prefractal interface. In this frame, it is shown that the properties of any generation prefractal can be deduced from the properties of the fractal generator, which are easy to reach numerically.

Keywords: Impedance; Model; Irregularity; Transport; Diffusion; Dirichlet-to-Neumann Operator.

1. INTRODUCTION

Transfer across irregular interfaces driven by Laplacian fields occurs in many different domains (electrochemistry, heterogeneous catalysis, NMR relaxation in porous media, transfer across biological membranes, etc.) In each of these situations, the physical transport properties of the system (through the bulk and across the interface) interplay in a complicated way with the geometrical characteristics of the interface, to give rise to a macroscopic response. A number of theoretical, numerical and experimental works have been devoted to this problem.[1–21]

Recently a rigorous solution of that question was given,[21] and in this paper we propose a simplified version of these results which can be used to understand the macroscopic response of deterministic self-similar interfaces. This model is formulated with the help of the "harmonic geometrical spectrum" deduced from the Dirichlet-to-Neumann operator.[19,21] It is based on a simplification of this spectrum obtained from a thorough numerical study of deterministic Koch curves and surfaces. The macroscopic response is derived in an explicit form for an arbitrary generation of the interface providing the correct behavior in two asymptotic limits (low and high frequencies) and approximate constant phase angle (CPA) behavior for intermediate frequencies. Its explicit form allows to study the crossover regions and the establishment of the CPA behavior with the generation order. The comparison with results of numerical simulations for the first four generations exemplifies the good accuracy of the model predictions.

The paper is organized as follows. In the next section, we briefly recall the "harmonic geometrical spectrum" approach based on the Dirichlet-to-Neumann operator. The hierarchical structure of these spectra is discussed in Sec. 3 for different Koch boundaries in two and three dimensions. A simplified analytical model of the macroscopic response is proposed. In Sec. 4, this model is generalized to the case of a deterministic prefractal interface.

2. THE DIRICHLET-TO-NEUMANN OPERATOR APPROACH

A basic picture of an electrolytic cell is constituted of a working electrode and a counter-electrode separated by an electrolyte with resistivity ρ. The electroneutrality, insured by the rapid motion of ions, leads to an electric potential V obeying the Laplace equation in the bulk. The amplitude V_0 of the applied potential is fixed at the counter-electrode. The other boundary condition is given by the charge conservation at the working electrode. On one hand, the density of the electric current from the electrolyte bulk is $\rho^{-1}\partial V/\partial n$, where $\partial/\partial n$ is the normal derivative on the metallic surface directed towards the bulk. One the other hand, the density of the electric current passing through the working electrode is $V/\zeta(\omega)$, $\zeta(\omega)$ being the surface impedance which may depend on the frequency ω. The charge conservation implies thus the mixed boundary condition at the working electrode:[15]

$$\begin{cases} V = V_0 & \text{on the counter-electrode} \\ \Delta V = 0 & \text{in the bulk} \\ \dfrac{\partial V}{\partial n} = \dfrac{V}{\Lambda} & \text{at the working electrode.} \end{cases} \tag{1}$$

The length Λ, defined as $\zeta(\omega)/\rho$, contains the relevant physical parameters about the system. For instance, in a linearized steady state regime, the surface impedance ζ is simply equal to the surface resistance r of the working electrode while for the purely capacitive regime, one has $\zeta(\omega) = (i\omega\gamma)^{-1}$, γ being the surface double layer capacitance.

A formal analogy allows to interpret these equations in a diffusional language: a "species" characterized by its concentration V diffuses in a bulk from a distant source (counter-electrode) towards a "semi-permeable" interface (working electrode), on which it disappears at a given rate (for instance, by transferring across the interface). In this case, the length Λ is defined as the ratio between the bulk diffusion coefficient D and the surface permeability $W : \Lambda = D/W$.[15]

Although one can numerically solve the system (1) for a given domain Ω (bulk), the influence of the geometry on the transport properties remains unrevealed in the present form. For a better understanding of the Laplacian transport phenomena, a "harmonic geometrical spectrum" approach had been recently developed.[21] In this section, we briefly outline its main features.

For a given diffusional or electrolytic cell Ω, one can introduce the Dirichlet-to-Neumann operator $\mathcal{M}$. This operator is defined as follows: if one considers a function f on the working interface $\partial\Omega$, this operator associates to f the normal derivative $\partial u/\partial n$, where u is the solution of the Laplace equation $\Delta u = 0$ in the bulk with the Dirichlet

boundary condition $u = f$ on $\partial\Omega$:

$$\mathcal{M}\ f = \frac{\partial u}{\partial n}. \tag{2}$$

For diffusional problems, the function f can be thought of as a given distribution of "species" on the working interface that have been sent to diffuse in the bulk Ω and then come back to this interface. Their flux density $\partial u/\partial n$ can thus be written as the application of the Dirichlet-to-Neumann operator $\mathcal{M}$ to the distribution f. In an electrochemical frame, one can consider the working interface $\partial\Omega$ with a given electric charge distribution f, and the application of the operator $\mathcal{M}$ to f provides the density of the induced electric field. From the mathematical point of view, the Dirichlet-to-Neumann operator is a pseudo-differential self-adjoint operator, characterized by a discrete positive spectrum and smooth eigenfunctions that form a complete basis of the space $L^2(\partial\Omega)$ of measurable and square integrable functions on $\partial\Omega$ (for mathematical details, see Refs. 22 and 23).

Once the Dirichlet-to-Neumann operator is defined for a given domain Ω, one can use it to characterize the macroscopic response of the working interface (Fig. 1). In particular, the flux or current density $\phi_\Lambda = \partial V/\partial n$ can be written as[21]

$$\phi_\Lambda = (I + \Lambda\mathcal{M})^{-1}\phi_0, \qquad \phi_0(s) = \rho^{-1}V_0[\mathcal{M}1](s)$$

where the specific flux density $\phi_0(s)$ corresponds to a perfectly conducting interface ($\Lambda = 0$). The admittance $Y(\Lambda)$ of the cell is defined to be proportional to the total current or flux Φ_Λ through the working interface: $Y(\Lambda) = \Phi_\Lambda/V_0$. This admittance can be exactly written as the spectral decomposition of the normalized flux density $\phi_0^n(s) = \phi_0(s)/\Phi_0$ over the eigenvectors $\mathbf{V}_\alpha$ of the Dirichlet-to-Neumann operator $\mathcal{M}$:[21]

$$Y(\Lambda) = \frac{\rho}{R^2}\sum_\alpha \frac{F_\alpha}{\mu_\alpha(1 + \Lambda\mu_\alpha)} \tag{3}$$

where $R = V_0/\Phi_0$ is the access resistance of the electrolyte. Here the eigenvalues μ_α of the operator $\mathcal{M}$ have the dimensionality of the inverse of a length, while the spectral components $F_\alpha = (\phi_0^n \cdot \mathbf{V}_\alpha)(\phi_0^n \cdot \mathbf{V}_\alpha^*)$ have the dimensionality of the inverse of an area.

The admittance $Y(\Lambda)$ characterizes the facility first to reach the working interface (bulk transport) and then to cross it (surface transfer). If the interface is perfectly absorbing ($\Lambda = 0$), the admittance accounts only for the bulk transport. The pure contribution of the working interface can be characterized by the difference between total fluxes Φ_0 and Φ_Λ: $Z(\Lambda) = V_0(\Phi_0 - \Phi_\Lambda)/\Phi_0^2$. This quantity has been shown to be an *intrinsic* characteristic of the working interface and called its *effective impedance*. It can also be written as a spectral decomposition with the help of (3):

$$Z(\Lambda) = \rho\Lambda\sum_\alpha \frac{F_\alpha}{(1 + \Lambda\mu_\alpha)}. \tag{4}$$

The explicit formula (4) provides the exact dependency of the experimentally measured quantity $Z(\Lambda)$ as a function of the physical parameters of the problem (Λ and ρ). Moreover, the geometrical irregularity is *completely* represented via the spectral characteristics μ_α and F_α of the Dirichlet-to-Neumann operator $\mathcal{M}$. Whatever the nature of the transport phenomena (stationary diffusion, electric transport, heterogeneous catalysis), the geometrical irregularity of the interface can be taken into account through a discrete set of real positive numbers μ_α and F_α. The distribution $F(\mu)$, which is a Dirac comb, can thus be called the "harmonic geometrical spectrum" of the working interface. In particular, the zeroth eigenvalue μ_0 is proportional to the inverse of the average distance between the working interface and the source. For the sake of simplicity, we will deal with an infinitely distant source, when $\mu_0 = 0$. In this case, F_0 is equal to the inverse of the total area of the working interface. The extension to the case of a source at finite distance is straightforward.[21]

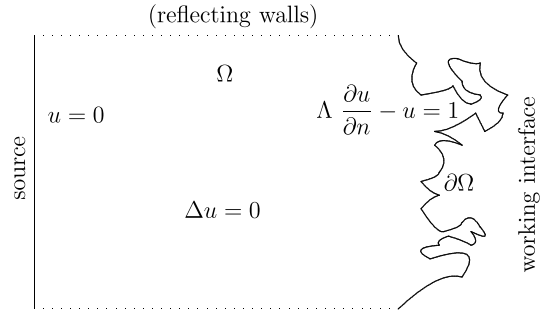

Fig. 1 In a typical diffusional cell, "species" diffuses in a bulk Ω from a distant source towards an irregular working interface $\partial\Omega$. This transport phenomenon can be seen as the mixed boundary value problem for the function u related to the concentration of species V as $V = V_0(1 - u)$.

3. HIERARCHY OF THE HARMONIC GEOMETRICAL SPECTRUM

Whatever the shape of the working interface, its accessibility for the particles diffusing from a distant source is characterized by the normalized flux density $\phi_0^n(s)$. In particular, the geometrical structure of the working interface should be represented somehow through the spatial distribution of this density. Being projected onto eigenvectors $\mathbf{V}_\alpha$ of the Dirichlet-to-Neumann operator, this density discriminates their contributions F_α to the macroscopic response. Since the eigenvectors $\mathbf{V}_\alpha$ oscillate along the working interface, one can expect that the most contributing eigenmodes correspond to the eigenvectors whose "spatial frequencies" are close to characteristic length scales of the working interface. Having the dimensionality of the inverse of a length, the corresponding eigenvalues μ_α appear as promising candidates to be related to these length scales. The numerical study of the quadratic Koch curve with a perfect hierarchy of characteristic length scales confirmed this hypothesis.[20]

3.1. Numerical Technique

For a given domain Ω, the Dirichlet-to-Neumann operator $\mathcal{M}$ can be numerically constructed in different ways. We used the approximation of the operator $\mathcal{M}$ by its discrete analog, the Brownian self-transport operator Q^a.[19,20] When the domain Ω is discretized by a lattice of mesh a, the Brownian self-transport operator is represented by a matrix composed of the probabilities $(Q^a)_{jk}$ for a random walker started from the boundary site j to reach the boundary site k at first hit without any contact with the interface or with the source during the walk. It had been pointed out that the Dirichlet-to-Neumann operator can be obtained in the continuous limit when the mesh parameter a vanishes: $(I - Q^a)/a \to \mathcal{M}$ as $a \to 0$.[24] The probabilistic meaning of the Brownian self-transport operator Q^a suggests different possibilities for its numerical calculation (Monte Carlo simulations, finite difference scheme, etc.). We used an appropriate modification of the boundary element method ascending to the (discrete) potential theory.[20] The practical implementation of our numerical method can be summarized as follows:

- for a given domain, one considers finer and finer discretizations with smaller and smaller mesh parameter a;
- for each discretization (each value of a), the Brownian self-transport operator Q^a is calculated;
- its eigenvalues q_α^a and eigenvectors $\mathbf{V}_\alpha^a$ are then computed by standard techniques; at the same time, the (discrete) normalized flux density $\phi_0^{n,a}$ is obtained;
- an approximation $\{\mu_\alpha^a, F_\alpha^a\}$ of the harmonic geometrical spectrum is constructed as:

$$\mu_\alpha^a = \frac{1 - q_\alpha^a}{a} \qquad F_\alpha^a = (\phi_0^{n,a} \cdot \mathbf{V}_\alpha^a)(\phi_0^{n,a} \cdot \mathbf{V}_\alpha^{*,a})$$

- for each α, the dependencies of μ_α^a and F_α^a as functions of the mesh parameter a are then extrapolated to the limit $a = 0$ that gives μ_α and F_α respectively.

This scheme was realized for several distances between the working interface and the source. In the case of an infinitely distant source, the Brownian self-transport operator Q^a can be constructed in a similar way, but the normalized flux density $\phi_0^{n,a}$ has to be approximated by that for a source at large but finite distance.

3.2. Quadratic Koch Curve

Finite generations of the quadratic Koch curve (of fractal dimension $\ln 5/\ln 3$) are probably the most convenient shapes to study the hierarchical structure of the harmonic geometrical spectrum. For deterministic prefractal interfaces, one can define a scaling homothety factor for both the perimeter (h_p) and the diameter (h_d) of the interface at each generation (for the quadratic Koch curve, $h_p = 5$ and $h_d = 3$). Being obtained iteratively from a simple shape (generator), these generations present a perfect hierarchy of characteristic length scales (Fig. 2). At the same time, the discretization of a domain comprised between the Koch curve and a planar source by a square lattice is straightforward. Note that, throughout this paper, the source was considered to be at infinite distance from the working interface.

The harmonic geometrical spectra for the first four generations of the quadratic Koch curve are shown in Fig. 3. Although the spectrum of the Dirichlet-to-Neumann operator is infinite, one could

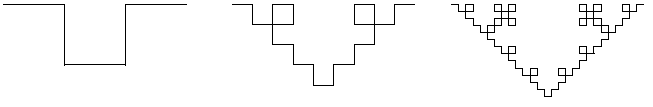

Fig. 2 First three generations of the quadratic Koch curve of fractal dimension $\ln 5/\ln 3$.

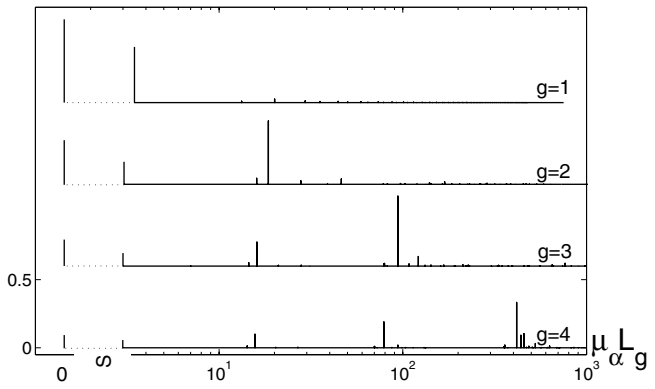

Fig. 3 Harmonic geometrical spectra $F_\alpha(\mu_\alpha)$ for the first four generations of the quadratic Koch curve of fractal dimension $\ln 5/\ln 3$ (the source is at infinity). To present the eigenvalue $\mu_0 = 0$ at logarithmic scale, the abscissa axis is interrupted. The eigenvalues are multiplied by the total perimeter L_g of the boundary.

expect only the eigenvectors with "spatial frequencies" smaller than the inverse of the smallest characteristic length to contribute to the macroscopic response. Consequently, the number of these eigenmodes might be expected to increase *exponentially* with generation order g. The main and striking observation from Fig. 3 is that the harmonic geometrical spectrum of the generation of order g contains mainly $(g + 1)$ eigenmodes contributing to the macroscopic response. As a consequence, the number of contributing eigenmodes increases *linearly* with g, or *logarithmically* with the smallest length of the interface. This observation drastically simplifies the analysis of the macroscopic response. Except for the eigenvalue μ_0 which is equal to 0, the eigenvalues corresponding to the contributing eigenmodes are equidistant at logarithmic scale; more precisely, the eigenvalues of two successive contributing eigenmodes differ by the scaling factor h_p of the perimeter (which is equal to 5 for this shape); in other words, the appearance of a new geometrical irregularity at a smaller length scale (next prefractal generation) is reflected in the harmonic geometrical spectrum by the single new eigenmode contributing to the macroscopic response.

Seeing how irregular the shape of the fourth generation is, the above results sound striking and even puzzling. What does make possible that among the infinity of the Dirichlet-to-Neumann operator eigenmodes, only a few specific ones contribute to the macroscopic response of the system? Why their positions on the logarithmic axis (eigenvalues μ_α) are equidistant?

To clarify these points, the projection of the eigenvectors $\mathbf{V}_\alpha$ to the normalized flux density ϕ_0^n has to be studied in detail. Let us first consider the case of a flat boundary (linear segment of length L). Since the random walkers coming from an infinitely remote source are uniformly distributed over the flat boundary, one gets $\phi_0^n(s) = 1/L$. The eigenvalues and eigenvectors of the Dirichlet-to-Neumann operator $\mathcal{M}$ are known explicitly:

$$\mu_\alpha = |\alpha|/L \qquad \mathbf{V}_\alpha(s) = L^{-1/2}\, e^{2\pi i \alpha s/L},$$

i.e. the eigenvectors $\mathbf{V}_\alpha$ form actually the Fourier basis, while the eigenvalues μ_α represent their spatial frequencies. It is now clear that the projection of any eigenvectors with $\alpha > 0$ onto the uniform density ϕ_0^n is strictly zero. The only contribution will be from the constant eigenvector $\mathbf{V}_0$ leading to $F_0 = 1/L$.

If the boundary is not flat, the normalized flux density $\phi_0^n(s)$ is not constant anymore, and the eigenbasis of the Dirichlet-to-Neumann operator is not formed by Fourier harmonics. However, the eigenvectors do still oscillate with increasing spatial frequencies, and the density $\phi_0^n(s)$ is still "smooth" at length scales smaller than the minimal cut-off of the irregular or prefractal interface (although it may possess integrable singularities at some boundary points). As a consequence, there is no contribution to the macroscopic response from highly oscillating eigenvectors. Let us consider as example the first generation of the Koch curve. The normalized flux density ϕ_0^n and several eigenvectors are shown in Fig. 4. We remind that there are two contributions. The first one, $F_0 = 1/L_g$, is due to the constant eigenvector $\mathbf{V}_0$, as in the case of a flat interface (here the perimeter $L_g = L(5/3)^g$ is equal to $L_1 = L(5/3)$). The new contribution F_1 comes from the eigenvector $\mathbf{V}_1$ "oscillating" at the spatial frequency of order of the inverse of the linear segment length $(L/3)$. Its projection onto the density ϕ_0^n leads to a non-trivial contribution. In particular, more rapid oscillations of the other eigenvectors cancel their contributions. A similar behavior is observed for the second, third and fourth generations of the Koch curve. In these cases, such a "resonance" effect is found not only at length scale $L/3$, but also at smaller scales: $L/3^2$ for $g = 2$, $L/3^2$ and $L/3^3$ for $g = 3$, etc. That explains the equidistant positions of the contributing peaks shown in Fig. 3. Their amplitudes progressively increase by a factor around 5/3 from the first peak to the last one (the trivial contribution

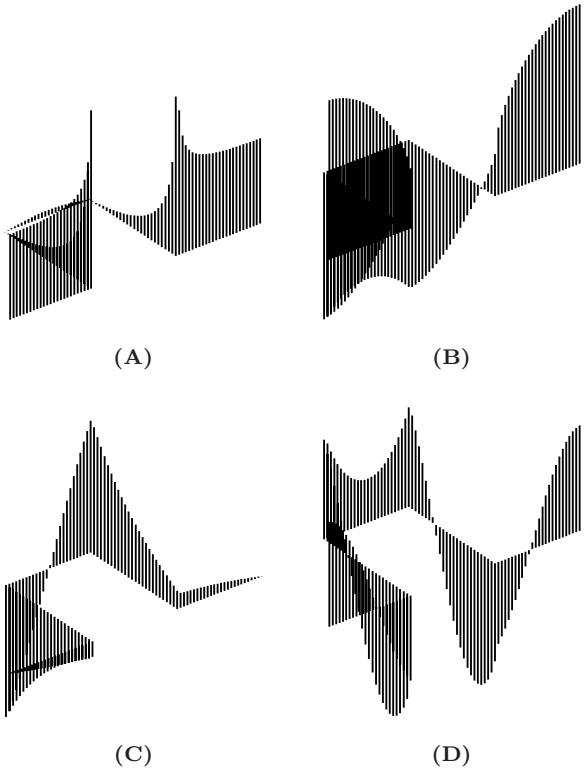

Fig. 4 Three-dimensional representation of the normalized flux density ϕ_0^n **(A)** and three eigenvectors $\mathbf{V}_\alpha$ [**(B)**, **(C)** and **(D)** for $\alpha = 1$, $\alpha = 2$ and $\alpha = 4$, respectively] for the first generation of the quadratic Koch curve of fractal dimension $\ln 5/\ln 3$. The trivial constant eigenvector $\mathbf{V}_0$ is not presented. A significant contribution comes from the scalar product between the normalized flux density ϕ_0^n and the eigenvector $\mathbf{V}_1$. The eigenvector $\mathbf{V}_2$ is anti-symmetric with respect to the density ϕ_0^n so that its contribution totally vanishes. In contrast, the eigenvector $\mathbf{V}_4$ is symmetric, but it does not almost contribute due to its oscillations.

F_0 of the flat interface is referred to as the 0th peak and will be considered separately). Indeed, the number of geometrical irregularities at length scale $L/3^{k+1}$ is mainly five times greater than that at length scale $L/3^k$, but they are three times smaller. Note that a little left shift of the peaks while passing successively from the first generation to the fourth may be caused by numerical uncertainty from the discretization procedure.

3.3. Analytical Model for the Quadratic Koch Curve

If $\mu_k^{(g)}$ and $F_k^{(g)}$ denote the positions and amplitudes of the peaks contributing to the macroscopic response of the quadratic Koch curve of generation g, the above observations can be translated into a simplified but rather faithful model

$$\mu_k^{(g)} L_g \simeq \begin{cases} m\ 5^k, & k > 0 \\ 0, & k = 0 \end{cases} \tag{5}$$

$$F_k^{(g)} L_g \simeq \begin{cases} f\ (5/3)^k, & k > 0 \\ 1, & k = 0 \end{cases} \tag{6}$$

where m and f are proportionality coefficients: $m \simeq 0.6$ and $f \simeq 0.4$. Knowing the coefficients m and f allows to reconstruct the harmonic geometrical spectrum for arbitrary generation order g, at least in a first approximation. In Table 1, we compare the numerical values of the positions and amplitudes of the contributing peaks for the first four generations with that given by our analytical

Table 1 Comparison Between the Main Contributing Peaks of the Harmonic Geometrical Spectra for the First Four Generations of the Quadratic Koch Curve of Fractal Dimension $\ln 5/\ln 3$ and the Model Scaling Relations for $\mu_k^{(g)}$ and $F_k^{(g)}$.

	g	$k=0$ ($\alpha=0$)	$k=1$ ($\alpha=1$)	$k=2$ ($\alpha=7$)	$k=3$ ($\alpha=37$)	$k=4$ ($\alpha=187$)
$\mu_\alpha L_g$	1	0	3.480			
	2	0	3.050	18.857		
	3	0	3.008	16.184	97.028	
	4	0	2.992	15.687	78.929	416.336
$\mu_k^{(g)} L_g$		0	3	15	75	375
$F_\alpha L_g$	1	1.000	0.686			
	2	1.000	0.463	1.335		
	3	1.000	0.441	0.822	2.545	
	4	1.000	0.437	0.772	1.465	2.573
$F_k^{(g)} L_g$		1.000	0.667	1.111	1.852	3.086

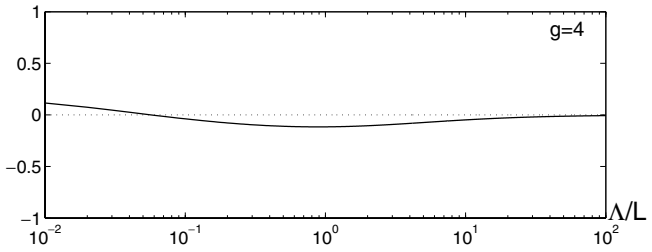

Fig. 5 Relative error of the model impedance $Z^{(4)}_{mod}(\Lambda)$ compared to the numerically computed impedance $Z(\Lambda)$ for the fourth generation of the quadratic Koch curve of fractal dimension $\ln 5/\ln 3$. This error is smaller than 12% for a wide range of values Λ.

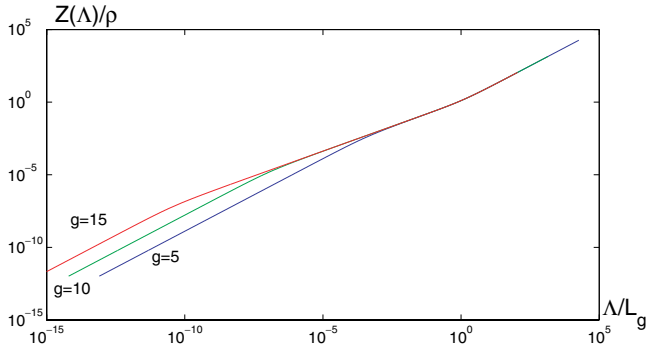

Fig. 6 The model impedance $Z^{(g)}_{mod}(\Lambda)$ for different generation orders g: 5, 10 and 15.

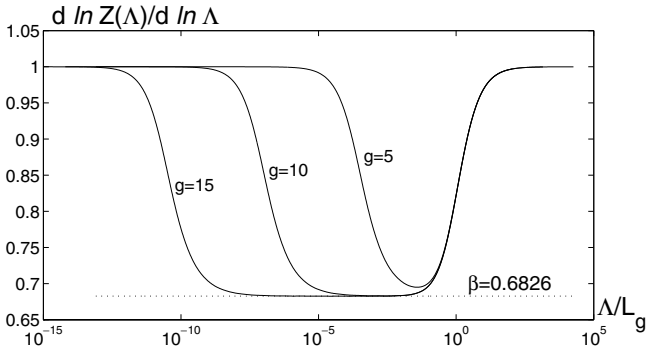

Fig. 7 Logarithmic derivative of the model impedance $Z^{(g)}_{mod}(\Lambda)$ for different generation orders g: 5, 10 and 15.

model (5) and (6). Although these values do not coincide exactly, they are reasonably close to each other. Moreover, the deviations between numerical and analytical values are less important for calculation of the effective impedance. Indeed, the effective impedance $Z(\Lambda)$ computed numerically from the exact spectral decomposition (4) has to be compared to the corresponding model impedance $Z^{(g)}_{mod}(\Lambda)$ defined as

$$Z^{(g)}_{mod}(\Lambda) = \rho\Lambda \sum_{k=0}^{g} \frac{F_k^{(g)}}{1+\Lambda\mu_k^{(g)}}. \qquad (7)$$

In contrast with the general relation (4), the only $(g+1)$ contributing eigenmodes are taken into account, and their positions $\mu_k^{(g)}$ and amplitudes $F_k^{(g)}$ are given by the analytical approximation (5) and (6). The comparison between $Z(\Lambda)$ and $Z^{(4)}_{mod}(\Lambda)$ for the fourth generation is shown in Fig. 5. The maximum relative error is 12% over five orders of magnitude of Λ/L. We conclude that the model impedance (7) captures the essential features of the macroscopic response. It is quite accurate for a wide range of values Λ even for the fourth generation of the quadratic Koch curve. At the same time, this model brings a drastic simplification of the problem since one now has an explicit analytical expression for an arbitrary fractal generation. In particular, the CPA behavior raised by a deterministic fractal morphology can be investigated (see the next section). It also provides an approximate but analytical description of the crossovers between the different regimes.

3.4. Macroscopic Response of High Generations

Given that our simplified analytical model has satisfactorily passed the numerical test for the first generations, the model impedance is now calculated for an arbitrary generation g. Figure 6 shows the model impedances for different generation orders g: 5, 10 and 15. One can distinguish two asymptotic limits with linear dependence on Λ, and an intermediate non-trivial behavior. To focus on the scaling exponent, the logarithmic derivative of the impedance with respect to Λ is plotted in Fig. 7. It converges to 1 at both asymptotic limits, Λ going to 0 and infinity. For the intermediate region, which becomes larger for higher generation orders, one can observe a plateau at a constant value of the impedance exponent β. The obtained numerical value $\beta \simeq 0.68$ is very close to the approximate value $1/D_f$ for this exponent.[5,6,10,15,18] The exact result of Halsey and Leibig[14] leads to a smaller value $\beta = \tau(2)/D_f$, $\tau(2)$ being the correlation dimension of the harmonic measure. We will return to this discussion in Sec. 4.2.

A general remark can be derived from the results shown in Fig. 7. As soon as the interface differs from a flat one, an intermediate region between two asymptotic limits is required to "link" two linear dependencies $\rho\Lambda/L_{act}$ and $\rho\Lambda/L_{tot}$ (since

the Dirichlet active zone length L_{act} is necessarily smaller than the total perimeter L_g due to diffusional screening). Figure 7 clearly shows that a well-established power law behavior can be reached only for sufficiently high generation orders. For example, the model impedance of the generation $g = 5$ does not yet exhibit such behavior. The crossovers play then a significant role if the fractal range is too narrow. In the same sense, the generation $g = 10$ exhibits already a well-established CPA behavior but only on four orders of magnitude for Λ. Most numerical simulations in the literature are done for the first four or five generations, which means that reported values of the impedance exponent must be handled with care.

3.5. Extension to Self-Similar Interfaces

The above arguments developed specifically for the quadratic Koch curve of fractal dimension $\ln 5/\ln 3$ can be extended to a large class of deterministic self-similar interfaces.

Let us consider the first generation (generator) of a deterministic self-similar interface. Although its harmonic geometrical spectrum is formally composed of infinite number of peaks characterized by pairs (μ_α, F_α), there is only a finite number of peaks contributing to the macroscopic response. This number depends on the geometrical complexity of a chosen interface. For the first generation (e.g. the generation) one would expect, as previously, one contribution $(\mu_0^{(1)}, F_0^{(1)})$ due to the constant eigenvector, and one or several contributions $(\mu_{1,j}^{(1)}, F_{1,j}^{(1)})$ from one or several length scales of the first generation. Here the superscript (1) denotes the generation order $g = 1$, while the subscript j enumerates different length scales ranging from 1 to J. For example, J was equal to 1 for the quadratic Koch curve studied in the previous subsections.

When passing to the second generation, one actually reproduces each of the above characteristic lengths at a smaller scale. Therefore, one may expect to appear $2J + 1$ contributing eigenmodes since there are $J + J$ characteristic length scales: the previous ones of the first generation, and those obtained by rescaling them. In general, the generation of order g would possess $gJ + 1$ peaks contributing to its macroscopic response: contribution of the constant eigenvector $(\mu_0^{(g)}, F_0^{(g)})$ and J sequences $(\mu_{k,j}^{(g)}, F_{k,j}^{(g)})$ of g peaks risen by g consecutive rescaling of J initial characteristic length scales.

The only difference with respect to the previous example of the quadratic Koch curve is that now there are possibly several sequences of equidistant peaks instead of the single one. And for each of these sequences, the scaling relations, similar to (5) and (6), are expected to hold. Indeed, two successive eigenvalues $\mu_{k,j}^{(g)}$ and $\mu_{k+1,j}^{(g)}$ (of the same sequence) differ by the homothety factor h_p of the perimeter that leads to

$$\mu_{k,j}^{(g)} L_g \simeq m_j (h_p)^k \tag{8}$$

where the coefficients m_j can be found numerically from the analysis of the first generation. The perimeter L_g of the generation g can be related to its diameter L by the scaling relation $L_g = (h_p/h_d)^g L$, h_d being the homothety factor of the diameter.

The arguments for the spectral components $F_{k,j}^{(g)}$ are quite similar. Indeed, the number of geometrical irregularities at scale of order $k + 1$ is h_p times greater than that of order k, but they are h_d times smaller. Consequently, two successive spectral components $F_{k,j}^{(g)}$ and $F_{k+1,j}^{(g)}$ (of the same sequence) differ by the ratio h_p/h_d, whence:

$$F_{k,j}^{(g)} L_g \simeq f_j (h_p/h_d)^k \tag{9}$$

where the coefficients f_j can be found numerically from the analysis of the first generation. Note that these scaling arguments do not pretend to mathematical rigorousness, but will be confirmed by numerical simulations in the next subsection.

The contribution of the zeroth eigenmode is

$$\mu_0^{(g)} = 0 \qquad F_0^{(g)} L_g = 1. \tag{10}$$

In the framework of this analytical model, the harmonic geometrical spectrum of prefractal interfaces is represented through their simple geometrical characteristics: the homothety factors h_p and h_d and the diameter L of the curve. The only empirical parameters that have to be calibrated are the coefficients m_j and f_j. For this purpose, it is sufficient to study the first generation and to compute numerically the contributing eigenmodes. That represents a drastic simplification of the problem.

3.6. Numerical Verification for Different Koch Interfaces

We have checked the above analysis for several Koch curves and surfaces (their generators are shown in

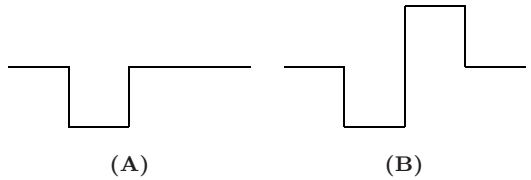

Fig. 8 Generators for two quadratic Koch curves of fractal dimensions $\ln 6/\ln 4$ **(A)** and $\ln 8/\ln 4$ **(B)**.

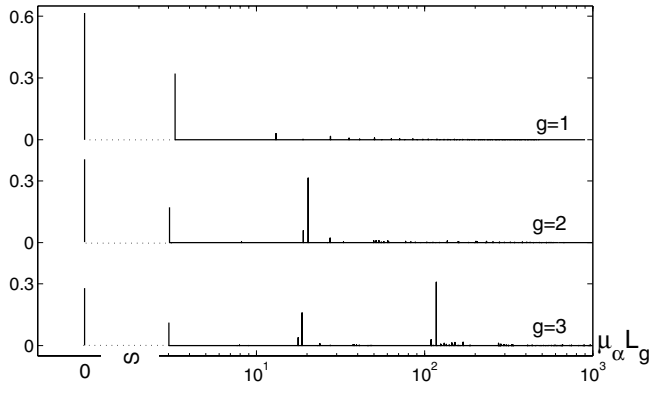

Fig. 9 Harmonic geometrical spectra $F_\alpha(\mu_\alpha)$ for the first three generations of the quadratic Koch curve of fractal dimension $\ln 6/\ln 4$.

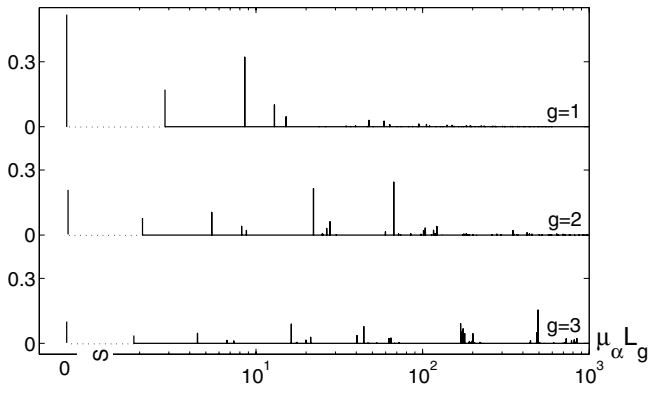

Fig. 10 Harmonic geometrical spectra $F_\alpha(\mu_\alpha)$ for the first three generations of the quadratic Koch curve of fractal dimension $\ln 8/\ln 4$.

Figs. 8 and 11). Since the calculation procedure and the analysis are essentially the same as for the previous case (Sec. 3.2), we only present the main results.

Figures 9 and 10 show the harmonic geometrical spectra for the first three generations of the quadratic Koch curves of fractal dimensions $\ln 6/\ln 4$ and $\ln 8/\ln 4$, respectively. In the first case ($h_p = 6$ and $h_d = 4$), one observes a single sequence of contributing peaks generated by the single characteristic length scale of this generator ($J = 1$).

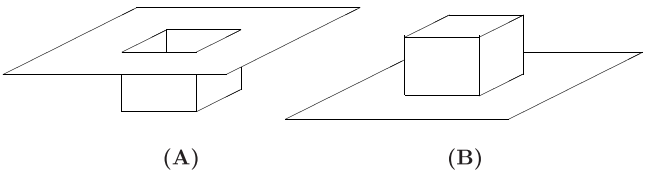

Fig. 11 Generators for two cubic Koch surfaces of fractal dimension $\ln 13/\ln 3$: concave **(A)** and convex **(B)**.

The eigenvalues $\mu_k^{(g)}$ are equidistant at logarithmic scale, while the corresponding spectral components $F_k^{(g)}$ differ by the factor h_p/h_d. The coefficients m and f are close to $1/2$ and $1/3$, respectively. Nothing special is found for this geometry with respect to the previously studied quadratic Koch curve of fractal dimension $\ln 5/\ln 3$.

In the second case ($h_p = 8$ and $h_p = 4$), a new feature is that there are two sequences of contributing peaks ($J = 2$), since the generator shown in Fig. 8B involves two characteristic length scales. As previously, each of these lengths is rescaled with the factor h_p leading to a linear shift of the corresponding peaks at logarithmic scale of Fig. 10. The coefficients m_j and f_j are found to be:

$$m_1 \simeq 1/4 \quad m_2 \simeq 1 \qquad f_1 \simeq 1/6 \quad f_2 \simeq 1/3.$$

As previously, some secondary peaks can be fused with the principal ones.

In principle, one can study the self-similar curves iterated from a more complex generator presenting three or more characteristic length scales. In practice, however, the identification of the corresponding scales may be technically difficult.

The numerical study of self-similar surfaces in 3D requires higher computational resources since an appropriate discretization leads to larger matrices representing the Brownian self-transport operator. For this reason, the harmonic geometrical spectra have been computed only for the first two generations of the concave and convex Koch surfaces of fractal dimension $\ln 13/\ln 3$ (their generators are shown in Fig. 11).

The harmonic geometrical spectra for both surfaces are shown in Fig. 12. The comparison between the first two generations suggests that, in both cases, there is a single characteristic length scale generating the single sequence of contributing peaks ($J = 1$). The coefficients m and f are found to be close to $4/9$ and $4/13$, respectively. The model impedance can be calculated for an arbitrary generation order using the geometrical parameters of these surfaces: $h_s = 13$,

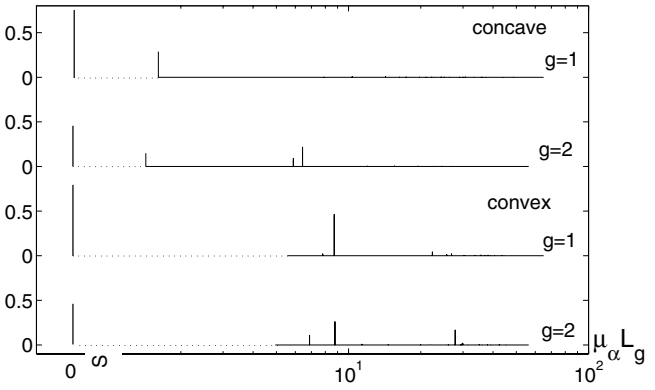

Fig. 12 Harmonic geometrical spectra $F_\alpha(\mu_\alpha)$ for the first two generations of two cubic Koch surfaces of fractal dimension $\ln 13/\ln 3$.

$h_d = 3$ and $h_p = 13/3$ (see the next section). An accurate simulation for the third generation would be helpful to validate the model for these Koch surfaces.

4. ANALYTICAL MODEL OF THE MACROSCOPIC RESPONSE

The scaling relations (8) to (10) allow to obtain the approximate but explicit formulae for the macroscopic response of the studied prefractal interface. For example, the effective impedance $Z(\Lambda)$ can be written as

$$Z^{(g)}_{mod}(\Lambda) = \rho \left[\frac{\Lambda}{L_g} + \sum_{j=1}^{J} \frac{f_j}{m_j}\, z(m_j \Lambda / L_g) \right] \qquad (11)$$

where the explicit function $z(x)$ only depends on the simple geometrical characteristics of the working interface:

$$z(x) = x \sum_{k=1}^{g} \frac{h_d^{-k}}{h_p^{-k} + x}. \qquad (12)$$

A similar expression can be written for the admittance $Y(\Lambda)$ of diffusional or electrolytic cell. Once the coefficients m_j and f_j are determined for the considered type of self-similar geometry, the relations (11) and (12) provide an approximate but explicit dependency of the effective impedance on the physical parameter Λ, *for any generation order g*.

4.1. CPA Behavior

The presence of different length scales ranging from the smallest geometrical features of the working interface up to its total perimeter leads to a non-trivial frequency dependence of the impedance largely deviating from the linear one. The most common dependence experimentally observed and numerically studied is called the constant phase angle (CPA) behavior, when the impedance as a function of Λ (or frequency) follows a power law in a certain range of values Λ:

$$Z(\Lambda) \simeq \rho\ (\Lambda/L)^\beta \qquad (13)$$

the exponent β lying between 0 and 1. In the Appendix, it is shown that the model impedance $Z^{(g)}_{mod}(\Lambda)$ exhibits this CPA behavior, provided that the generation g is sufficiently large. In particular, the exponent β is related to the homothety factors h_p and h_d:

$$\beta = \frac{\ln h_d}{\ln h_p} = \frac{1}{D_f}. \qquad (14)$$

Within this model, one captures the essential features of the macroscopic response of an irregular interface with self-similar hierarchical structure. The relation (14) between the impedance exponent β and fractal dimension D_f had been derived by different methods (general scaling arguments, dimension analysis, etc.)[3–6,10,15,18,25] The main advantage of the present approach is the *explicit* dependence of the model impedance on the physical parameter Λ.

4.2. Correlation Dimension

The relation (14) between the impedance exponent β and fractal dimension D_f is known as an approximation. A detailed scaling analysis performed by Halsey and Leibig[14] led to a slightly different expression involving the correlation dimension $\tau(2)$ of the harmonic measure on the working interface in 2D:

$$\beta = \frac{\tau(2)}{D_f}. \qquad (15)$$

This dimension allows to account for a multifractal scaling behavior of the hitting probabilities near geometrical singularities. The extensive studies of the harmonic measure on different fractal curves in the plane showed that the correlation dimension is relatively close to 1, taking in general values comprised between 0.85 and 0.95.[21,26–32] It is not thus surprising that such a subtle behavior of the harmonic measure is not taken into account by the

present model, which only involves simple geometrical features as scaling homothety factors. A further numerical study of the spectral properties of the Dirichlet-to-Neumann operator would permit to link the features that have been neglected in the approximate harmonic geometrical spectrum to the correlation dimension in the real scaling limit.

4.3. Extension to 3D Case

The preceding analysis can be easily extended to self-similar surfaces defined by the homothety factor h_d of the diameter and the homothety factor h_s of the surface. The "perimeter" of such a surface can then be introduced in a classical way as the surface area divided by the diameter. The corresponding homothety factor h_p is then equal to h_s/h_d. This definition is logically consistent with the scaling relations (8) and (9) for the harmonic geometrical spectrum. For instance, the ratio between two successive weights $F^{(g)}_{k+1,j}$ and $F^{(g)}_{k,j}$ is h_s/h_d^2, since the number of new (smallest) irregularities is h_s times greater, but their "strength" is h_d^2 times smaller. The model impedance can thus be written as

$$Z^{(g)}_{mod}(\Lambda) = \rho \left[\frac{\Lambda}{S_g} + \frac{L_g}{S_g} \sum_{j=1}^{J} \frac{f_j}{m_j}\, z(m_j \Lambda / L_g) \right]$$

where S_g is the total surface area of the generation g, $S_g = (h_s/h_d^2)^g L^2$; L_g is its perimeter, $L_g = S_g/L = (h_s/h_d^2)^g L$, while the function $z(x)$ remains unchanged. Consequently, one can apply the same analysis for this model impedance. In particular, the substitution of h_p into (14) gives

$$\beta = \frac{1}{D_f - 1}$$

in agreement with other approaches, for which $D_f = \ln h_s / \ln h_d$.

4.4. Realistic Interfaces

Deterministic hierarchical scaling of self-similar boundaries is difficult to find in nature or industrial frames, where *randomness* and *variability* are generally present. But the deterministic self-similar surfaces can be thought of as a simplifying paradigm of more realistic irregular interfaces.[33] For example, it has been shown that the macroscopic response of fractal curves in 2D essentially depends on their dimension and little on the deterministic or random character of their geometry.[34] This means that their transport properties are determined more by their hierarchical structure than by a specific geometrical arrangement. In this light, *the model impedance derived in this paper is expected to describe approximately the properties of many realistic morphologies.*

The idea is the following. Whether an irregular curve is fractal or not, one can define its "effective" fractal dimension as

$$\hat{D}_f = \frac{\ln(L_{tot}/\ell)}{\ln(L/\ell)}$$

where L_{tot} and L are the perimeter and diameter of this curve, while ℓ is the smallest cut-off which is naturally determined by specific features of the studied transport phenomena (e.g. it can be the size of catalytic germs in chemical industry). According to Filoche and Saporal,[34] in 2D the macroscopic response of this irregular curve is close to that of a deterministic fractal of the same fractal dimension. Thus, if one builds such a deterministic fractal (for instance, a Koch curve), its analytical impedance model can be used to represent also the impedance of the former irregular boundary. Furthermore, since the model impedance integrates information about the positions and the amplitudes of the contributing eigenmodes (4), it implicitly yields some information about the density and the contributions of the eigenmodes of the irregular or random interface as well, *whatever its geometrical complexity.* Since the model impedance is found in an explicit analytical form, the whole range of frequencies (or Λ) can be investigated, including the crossover regions. A further numerical study will be valuable to develop this concept for different natural interfaces.

5. CONCLUSION

In this paper, we have developed an analytical model describing the macroscopic impedance of deterministic self-similar interfaces. This model is based on a mathematical solution of the Laplacian transport using the properties of the Dirichlet-to-Neumann operator. The effective impedance is derived in an analytical form, in which the geometry is represented by a set of spectral characteristics of this operator referred to as its "harmonic geometrical spectrum." In the case of deterministic self-similar boundaries, the spectrum can be simplified due to its hierarchial structure which in turn results from self-similarity of the interface. As each

characteristic length scale of the generator produces a sequence of contributing peaks to the harmonic geometrical spectrum, simple scaling relations can be deduced for these characteristics. The prefactors remain unknown but they may be calibrated by numerical simulations of the Laplacian transport in the *elementary generator only* and such simulations are in general easy to realize. Once these coefficients are determined, one can use the explicit relation for the model impedance for any prefractal generation. The impedance exponent β of the CPA behavior is found to be related to the fractal dimension of the working interface. An explicit formula allows to study the crossover regions between the asymptotic limits and the CPA regime which is shown to exist only for large generation order prefractals. It clearly indicates that the first generations exhibit rather some sort of transitional behavior at the intermediate region instead of showing a proper CPA behavior.

The model assumptions and predictions have been carefully checked in 2D for quadratic Koch boundaries of different fractal dimensions. The comparison between the model impedance and the numerically computed impedance even for the fourth generation showed that the maximum relative error is less than 12% for all values of Λ. It indicates that the model impedance captures the essential features of the macroscopic response both in qualitative and quantitative senses. Since it is known that the response of random and deterministic fractals of the same fractal dimension are very similar, this study opens the way for a better understanding of the "harmonic geometrical spectrum" of random fractal interfaces.

Further developments should include a careful check of the approximate model for prefractal surfaces in 3D and an explanation on how the correlation effects of the harmonic measure intervene in the spectral formalism of this problem.

REFERENCES

1. R. de Levie, *Electrochim. Acta* **10** (1965) 113–130.
2. R. D. Armstrong and R. A. Burnham, *J. Electroanal. Chem.* **72** (1976) 257–266.
3. A. Le Méhauté and G. Crepy, *C. R. Acad. Sci. II Paris* **294** (1982) 286–288.
4. A. Le Méhauté, A. de Guibert, M. Delaye and C. Filippi, *C. R. Acad. Sci. II Paris* **294** (1982) 835–837.
5. L. Nyikos and T. Pajkossy, *Electrochim. Acta* **30** (1985) 1533–1540.
6. P. Meakin and B. Sapoval, *Phys. Rev. A* **43** (1991) 2993–3004.
7. S. H. Liu, *Phys. Rev. Lett.* **55** (1985) 529–532.
8. M. Keddam and H. Takenouti, *C. R. Acad. Sci. II Paris* **302** (1986) 281–284.
9. M. Keddam and H. Takenouti, *Electrochim. Acta* **33** (1988) 445–448.
10. B. Sapoval, R. Gutfraind, P. Meakin, M. Keddam and H. Takenouti, *Phys. Rev. E* **48** (1993) 3333–3344.
11. R. de Levie, *J. Electroanal. Chem.* **261** (1989) 1–9.
12. R. de Levie, *J. Electroanal. Chem.* **281** (1990) 1–21.
13. T. C. Halsey, *Phys. Rev. A* **35** (1987) 3512–3521.
14. T. C. Halsey and M. Leibig, *Ann. Phys.* **219** (1992) 109–147.
15. B. Sapoval, *Phys. Rev. Lett.* **73** (1994) 3314–3316.
16. J. Gunning, *J. Electroanal. Chem.* **392** (1995) 1–11.
17. B. Sapoval, in *Fractals and Disordered Systems*, eds. A. Bunde and S. Havlin (Springer, 1996), pp. 233–261.
18. B. Sapoval, M. Filoche, K. Karamanos and R. Brizzi, *Eur. Phys. J. B* **9** (1999) 739–753.
19. M. Filoche and B. Sapoval, *Eur. Phys. J. B* **9** (1999) 755–763.
20. D. S. Grebenkov, M. Filoche and B. Sapoval, *Eur. Phys. J. B* **36** (2003) 221–231.
21. D. S. Grebenkov, M. Filoche and B. Sapoval, *Phys. Rev. E* **73** (2006) 021103–1–9.
22. M. S. Agranovich, in *Partial Differential Equations IX*, ed. M. S. Agranovich, Yu. V. Egorov and M. S. Shubin (Springer, 1997) EMS79.
23. M. S. Birman and M. Z. Solomyak, *Spectral Theory of Self-Adjoint Operators in Hilbert Space* (D. Reidel Publishing Company, 1987).
24. D. S. Grebenkov, in *Focus on Probability Theory*, ed. L. R. Velle (Nova Science Publishers Inc., 2006), pp. 135–169.
25. D. S. Grebenkov, *Fractals* **14** (2006) 231–243.
26. P. Meakin, *Phys. Rev. A* **33** (1986) 1365–1371.
27. M. H. Jensen, A. Levermann, J. Mathiesen and I. Procaccia, *Phys. Rev. E* **65** (2002) 046109–1–8.
28. D. S. Grebenkov, *Phys. Rev. Lett.* **95** (2005) 200602–1–4.
29. M. Leibig and T. C. Halsey, *J. Electroanal. Chem.* **358** (1993) 77–109.
30. H. Ruiz-Estrada, R. Blender and W. Dieterich, *J. Phys. Condens. Matter* **6** (1994) 10509–10517.
31. B. Duplantier, *Phys. Rev. Lett.* **82** (1999) 3940–3943.
32. D. S. Grebenkov, A. A. Lebedev, M. Filoche and B. Sapoval, *Phys. Rev. E* **71** (2005) 056121–1–11.
33. B. Sapoval, *Universalités et Fractales* (Flammarion, Paris, 1997).
34. M. Filoche and B. Sapoval, *Phys. Rev. Lett.* **84** (2000) 5776–5779.

APPENDIX

In this Appendix, we are going to show that the model impedance $Z_{mod}^{(g)}(\Lambda)$ exhibits the CPA behavior (13), provided that the generation order g is sufficiently high. In this case, one may expect that, for the intermediate values of Λ, the dominating contribution will be brought by the "intermediate" terms in the sum (12) over k. In order to determine this contribution, we write the function $z(x)$ by introducing the following notations: $\alpha_d = \ln h_d$ and $\alpha_p = \ln h_p$:

$$z(x) = x \sum_{k=1}^{g} \frac{e^{-\alpha_d k}}{e^{-\alpha_p k} + x}.$$

The largest contribution will correspond to k_0th term such that

$$\frac{d}{dk} \frac{e^{-\alpha_d k}}{e^{-\alpha_p k} + x} = 0$$

whence

$$k_0 = -\frac{\ln x\eta}{\alpha_p} \qquad \eta = \frac{\alpha_d}{\alpha_p - \alpha_d}.$$

For further analysis, it is convenient to rewrite the previous sum as

$$z(x) = x^{\alpha_d/\alpha_p} \eta^{\alpha_d/\alpha_p} \sum_{k=1}^{g} \frac{e^{-\alpha(k-k_0)}}{\eta e^{-\alpha_p(k-k_0)} + 1}. \quad (16)$$

One can now consider different cases:

- if $\eta e^{-\alpha_p(k-k_0)} \ll 1$ for any $k = 1, \ldots, g$, this term can be omitted in the denominator that leads to
$$z(x) = \frac{1 - e^{-\alpha_d g}}{e^{\alpha_d} - 1} = \frac{1 - (1/h_d)^g}{h_d - 1}$$
i.e. the constant term at the asymptotic limit of low frequencies. Written for $k = 1$, the above inequality gives $x \gg 1/h_p$.
- if $\eta e^{-\alpha_p(k-k_0)} \gg 1$ for any $k = 1, \ldots, g$, the unity can be omitted in the denominator that leads to
$$z(x) = x \frac{1 - (h_p/h_d)^g}{h_d/h_p - 1}$$
i.e. a linear proportionality at the asymptotic limit of high frequencies. Written for $k = g$, the above inequality gives $x \ll (1/h_p)^g$.
- In the intermediate case $(1/h_p)^g \ll x \ll 1/h_p$, the main contribution is given by terms with k around k_0, since the others terms exponentially decrease with $|k - k_0|$. This leads to a power law dependence of the function $z(x)$ on x:
$$z(x) \propto x^{\alpha_d/\alpha_p}$$
where the prefactor can be calculated numerically from (16). Since x is proportional to Λ, one deduces the CPA behavior of the model impedance $Z_{mod}^{(g)}(\Lambda)$ with exponent
$$\beta = \frac{\alpha_d}{\alpha_p} = \frac{1}{D_f}$$
where D_f is the fractal dimension of the considered self-similar curve, $D_f = \ln h_p / \ln h_d$.